Electrical Engineering in Japan, Vol. 165, No. 1, 2008
Translated from Denki Gakkai Ronbunshi, Vol. 127-D, No. 2, February 2007, pp. 139–145

Principle and Basic Characteristics of Linear Synchronous Motor with Half-Wave Rectified Self Excitation

TADASHI HIRAYAMA, JUN OYAMA, TSUYOSHI HIGUCHI, and TAKASHI ABE
Nagasaki University, Japan

SUMMARY

This paper presents the principle and basic characteristics of a novel linear synchronous motor based on "half-wave rectified self excitation principle." The field winding is short circuited through a diode and the armature winding consists of conventional three-phase windings. If the amplitude of the balance three-phase currents is modulated by an alternating wave with bias frequency, the produced magnetomotive force pulsates at the bias frequency and moves at the synchronous velocity. This pulsating magnetomotive force induces the electromotive force with a bias frequency in the field winding. The field excitation is obtained by rectifying the electromotive force with the diode in the field winding. In this paper, the authors design and build an experimental machine and confirm its basic characteristics. They also deduce the performance equations and investigate the thrust ripple reduction. © 2008 Wiley Periodicals, Inc. Electr Eng Jpn, 165(1): 82–90, 2008; Published online in Wiley InterScience (www.interscience.wiley.com). DOI 10.1002/eej.20684

Key words: linear synchronous motor; half-wave rectified; self-excitation; field weakening operation.

1. Introduction

The use of linear motors in the field of transport and conveyance continues to evolve, and combinations of linear induction motors (LIM) and linear synchronous motors (LSM) using magnetic levitation guidance or wheel support guidance have been developed. In the field of transport, linear motor subways in Tokyo, Osaka, Kobe, and Fukuoka, and the HSST in Nagoya, all propelled by LIMs, have been put into use [1, 2]. However, such motors in principle have a low power factor and efficiency, and improving them is problematic. In the field of conveyance, the speed, cleanness, and ease of maintenance of linear motors have led to conveyance systems using them as the drive source being developed for conveyance in hospitals, conveyance in clean rooms, and in sorting machines. In these conveyance devices, an LIM with the advantages of a conventional high-speed drive has primarily been used, but given the demands for greater positioning precision, there is a trend toward moving to LSM servo control [3]. Permanent magnet-type LSMs have become common in recent years given the improved performance and reduced cost of rare earth permanent magnets. However, in a permanent magnet-type LSM (PM-LSM), the magnet field flux is constant, and weakens during high-speed operation. For a magnetic field drive, an important issue is the need to control the d-axis current to cancel out the flux from the permanent magnets.

Thus, the authors have proposed a new LSM, their "lineary synchronous motor with half-wave rectified self-excitation," for transport and conveyance, which can freely control the field flux and does not require a power source or permanent magnet on the field side and is more efficient than an LIM [4]. The proposed new LSM consists of a conventional armature side with a three-phase armature winding, and a field side with a field winding that is short-circuited in a single phase using a diode. By supplying to the armature winding a pulsating current which superimposes the excitation current component on the thrust current component, the authors have created an alternating magnetomotive force which moves in synchronization with the mover d axis while pulsating at the bias frequency. This alternating magnetomotive force induces the electromotive force with bias frequency in the field winding. The field excitation is obtained by rectifying the electromotive force with the diode of the field winding [5]. The proposed new LSM does not require a power source because of the excitation on the field side, compared with a PM-LSM, and is structurally stronger and easier to maintain. Moreover, as is the case with permanent magnets, it also has the advantages of not demagnetizing or having its characteristics deteriorate because of an increase in tem-

perature. Because excitation of the field side is performed on the armature side, in a linear motor with a larger gap, the efficiency is lower compared to that of a PM-LSM. However, in field weakening operation at higher speeds, compared to a PM-LSM which requires providing d-axis current at all times because of demagnetization even at low propulsion levels, the new LSM can reduce the magnetic field flux by decreasing the amplitude of the excitation current component supplied to the armature, and so can operate in a field weakening operation without causing a loss of efficiency. When using the proposed new LSM in a short-armature-type transport system, setting up in the iron core on the ground the field side which has a field winding short circuited in single phase using a diode is sufficient. The new LSM can also be used in the acceleration section alone, which is a problem because of low efficiency, with a current linear motor subway car, primary side, and inverter being used as is.

In order to confirm the basic operation of the proposed new LSM, the authors designed a long-armature-type new LSM and created it [6, 7]. In this paper the authors first describe the principle and experimental setup for their newly proposed LSM, and then its basic characteristics. They then derive a characteristics equation for the LSM for use in design and control, and compare the calculated values with measured values. Finally, they consider a method to reduce the thrust ripple using their derived characteristics equation.

2. A Linear Synchronous Motor with Half-Wave Rectified Self-Excitation

2.1 Structure of the LSM

Figure 1 shows the structure of the long-armature-type linear synchronous motor with half-wave rectified self-excitation. This LSM consists of a mover with a field winding short circuited in one phase using a diode and a stator with a conventional three-phase armature winding. The LSM is driven using a voltage-type PWM inverter which generates three-phase alternating current based on the half-wave rectified self-excitation principle and in synchronization with the mover position.

2.2 dq-axis model

Figure 2 shows the dq-axis model for the LSM. The voltage equation for the dq axis and field winding can be written as follows:

$$\begin{aligned} e_d &= p\lambda_d - \omega\lambda_q + r_a i_d \\ e_q &= p\lambda_q + \omega\lambda_d + r_a i_q \\ e_{fd} &= p\lambda_{fd} + r_{fd} i_{fd} \end{aligned} \tag{1}$$

The flux linkages can be written as follows:

$$\begin{aligned} \lambda_d &= L_d i_d + M_{fd} i_{fd} \\ \lambda_q &= L_q i_q \\ \lambda_{fd} &= M_{fd} i_d + L_{fd} i_{fd} \end{aligned} \tag{2}$$

Here, e_d and e_q represent the dq axis voltage; e_{fd}: the field winding voltage; i_d and i_q: the dq axis current; i_{fd}: the field winding current; λ_d and λ_q: the dq axis winding flux linkage; λ_{fd}: the field winding flux linkage; r_a: the armature winding resistance; r_{fd}: the field winding resistance; L_d and L_q: the dq axis winding self-inductance; L_{fd}: the field winding self-inductance; M_{fd}: the mutual inductance between the d axis winding and field winding; ω: synchronous angular velocity; p: the differential operator.

2.3 Principles of self-excitation and thrust generation

The following three-phase AC current is provided in synchronization with the mover position to the three-phase armature winding in the LSM.

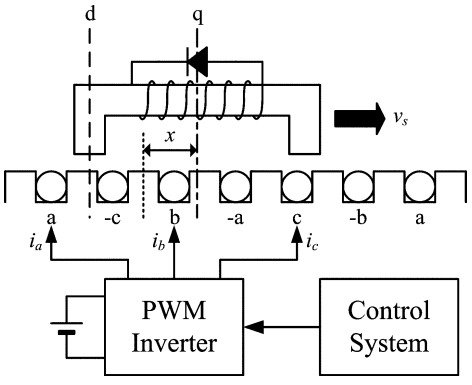

Fig. 1. Configuration of LSM.

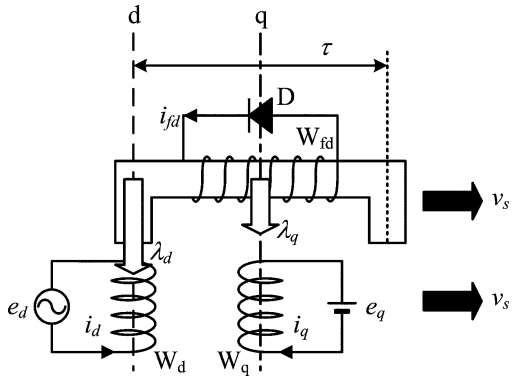

Fig. 2. Equivalent model on the dq axis.

$$
\begin{aligned}
i_a &= A_f(t)\sin\theta + \sqrt{2}I_t\cos\theta \\
i_b &= A_f(t)\sin(\theta - 2\pi/3) + \sqrt{2}I_t\cos(\theta - 2\pi/3) \\
i_c &= A_f(t)\sin(\theta - 4\pi/3) + \sqrt{2}I_t\cos(\theta - 4\pi/3)
\end{aligned} \tag{3}
$$

Here, $\theta = \pi x/\tau$ and x represent the mover position; τ: the pole pitch; the mover position x is taken to be $x = 0$ where the position of the stator a phase and q axis matches.

The first term on the right-hand side of Eq. (3) is excitation current, which varies with sine of the mover position and whose amplitude is modulated by a function $A_f(t)$, where $A_f(t)$ is a triangular wave function with the effective value of I_f and bias frequency ω_b. The second term of the right-hand side of Eq. (3) is thrust current component with the effective value of I_t. Figure 3 shows the waveforms for the $A_f(t)$, the excitation current component $A_f(t)\sin\theta$, the thrust current component $I_t\cos\theta$, and the a phase current i_a.

By converting Eq. (3) into the dq axis which moves synchronously with the mover position, the d-axis and q-axis currents become

$$
\begin{aligned}
i_d &= \sqrt{(3/2)}A_f(t) \\
i_q &= \sqrt{3}I_t
\end{aligned} \tag{4}
$$

The dq axis current i_d and i_q take the waveforms shown in Fig. 3. A pulsating magnetomotive force as obtained when the d axis current i_d in Eq. (4) is flowing through the d axis single phase winding W_d in Fig. 2 is

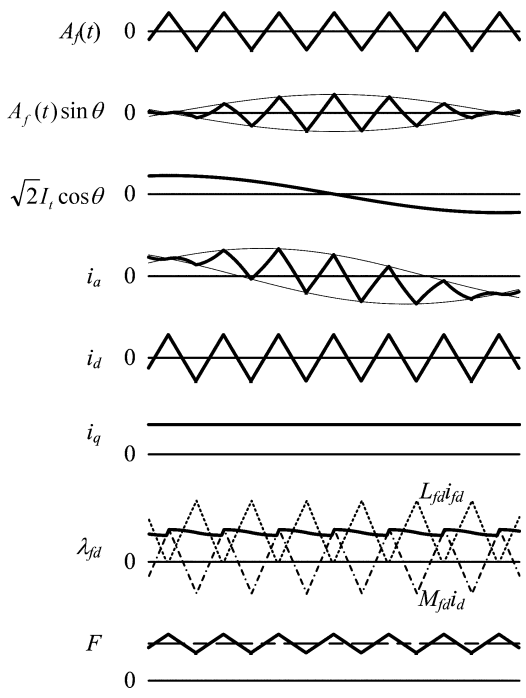

Fig. 3. Waveforms for current, flux, and thrust.

generated. In other words, the flux linkage $M_{fd}i_d$ pulsating at the bias frequency appears on the mover d axis.

The diode D inserted in the field winding is off when the flux linkage with the field winding rises. However, it is on when the flux falls. It operates so that the field current i_{fd} flows so as to maintain the peak value of the flux linkage with the field winding. In other words, the field current i_{fd} flows so as to maintain a maximum value for $M_{fd}i_d$. As a result, the field winding flux linkage λ_{fd} excites an almost constant flux as shown in Fig. 3. Here, by using a triangular wave, the effective value of the excitation current compared to a sine wave can be reduced for the modulated waveform $A_f(t)$ for the excitation current component, and the power factor and efficiency can be improved [8].

Next, when the q axis current i_q in Eq. (4) flows through the q axis single phase winding W_q in Fig. 2, the thrust generated by the LSM can be expressed as

$$
F = \frac{\pi}{\tau}(\lambda_d i_q - \lambda_q i_d) \tag{5}
$$

Moreover, when the field winding resistance is ignored, the thrust is as follows:

$$
F = \frac{\pi}{\tau}\left\{3\sqrt{\frac{3}{2}}(1-\sigma)L_d I_f I_t + \frac{3}{\sqrt{2}}(\sigma L_d - L_q)A_f(t)I_t\right\} \tag{6}
$$

Here, σ represents the leakage coefficient, and is given by

$$
\sigma = 1 - M_{fd}^2/(L_d L_{fd}) \tag{7}
$$

The first element on the right-hand side of Eq. (6) represents the average thrust, and the second element on the right-hand side represents the component pulsating with a modulated waveform $A_f(t)$. As such, in this LSM the pulsating thrust with the bias frequency ω_b as the base wave is included, and selecting ω_b and $(\sigma L_d - L_q)$ as appropriate does not present problems in practice.

3. Experimental Machine

3.1 Experimental machine

Figure 4 shows the general shape and dimensions of the prototype LSM, and Table 1 lists the design parameters. The prototype LSM is the long armature type, with a three-phase armature winding along the entire 2-m length of the stator. The mover has four poles, with a field winding set up at each pole. These are connected in series and inserted into the diode. The air gap between the stator and the mover is 0.6 mm. Figure 5 shows the external appearance of the experimental machine. The mover hangs from the track frame via a linear guide. Also, an optical scale sensor with a resolution of 0.1 mm is used to detect the

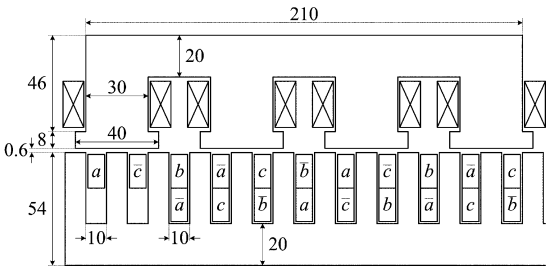

Fig. 4. Dimensions of the experimental machine (unit: mm).

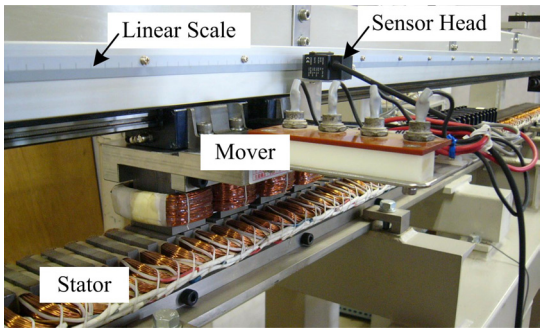

Fig. 5. Outline of the experimental machine.

position of the mover. A sensor head is attached to the mover, and a scale is attached to the track frame which guides the mover.

3.2 Drive system

Figure 6 is a diagram of the drive system configuration. This drive system is composed of an inverter system consisting of a voltage-type PWM inverter and a current tracking-type PWM signal generator that drives it, and a DSP control system.

In the DSP control system, the mover position information is input to the DSP, the measured velocity of the mover is calculated based on this position information, and a thrust current amplitude command is generated by PI control between the mover measured velocity and the command velocity input from the monitor PC. Moreover, a triangular wave $A_f(t)$ is created from the bias frequency command and the excitation current effective value command input from the monitor PC. Conversion from two phases to three phases is performed, and the three-phase current command value is output using the D/A converter. The above process is performed every 100 μs (10 kHz) using interrupts.

The three-phase current command value is compared with the real current obtained from the current sensor connected to each output terminal in the inverter, 5 μs of dead time is added, an IGBT control current tracking-type PWM signal is created in the inverter and input to the gate drive circuit.

Table 1. Design parameters of the experimental machine

Item		Value [Unit]
Stator length		1990 [mm]
Stack Height		50 [mm]
Pole Pitch		60 [mm]
Air Gap		0.6 [mm]
Rated Current		4 [A]
Number of Turns	Stator	85 [turn/pole]
	Mover	300 [turn]
Windings		Double Layer Distribution Pitch
Number of Poles		4
Resistance	Stator	9.9 [Ω]
	Mover	8.8 [Ω]
Weight of mover		11.15 [kg]

4. Basic Characteristics of the Experimental Machine

4.1 Drive characteristics of the experimental machine

The authors ran their experimental machine using the drive system in the previous section. Figure 7 shows the d

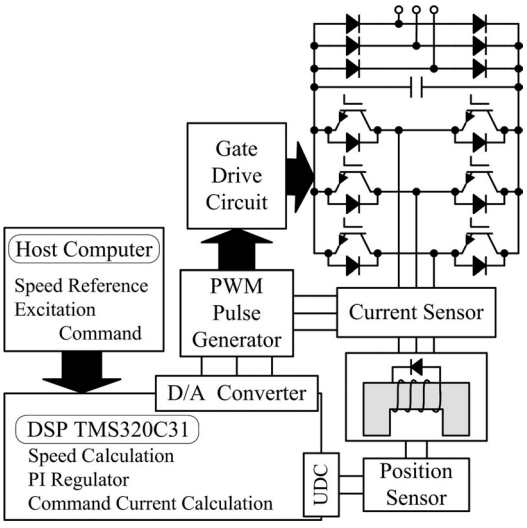

Fig. 6. Driving system configuration.

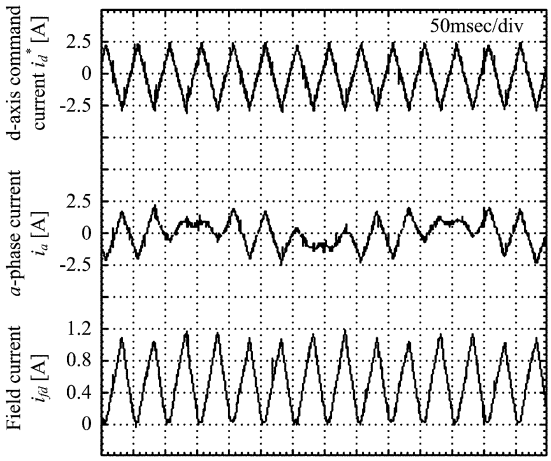

Fig. 7. Current waveforms.

axis command current i_d^*, the a phase real current i_a, and the field winding current i_{fd} for a velocity of 0.3 m/s, an excitation current effective value command I_f = 1.2 A, and a bias frequency of 20 Hz. As can be seen in Fig. 7, the field winding current waveform takes the theoretical shape given in Section 2, and the half-wave rectified self-excitation is performed as described.

Figure 8 shows the velocity response waveform for a round trip. The command velocity is varied in steps from 0.5 m/s to –0.5 m/s or –0.5 m/s to 0.5 m/s when the mover arrives at the return point. The conditions here are I_f = 1.2 A and a bias frequency of 20 Hz. As can be seen in the figure, the drive nicely follows the command, though the trajectory is simple.

4.2 Static thrust characteristics

Figure 9 shows the results of measuring the static thrust and position characteristics. For the static thrust, the mover is pushed against the compression load cell, the mover position is changed, and a measurement is taken at 1-mm intervals up to 20 mm, the displacement for one

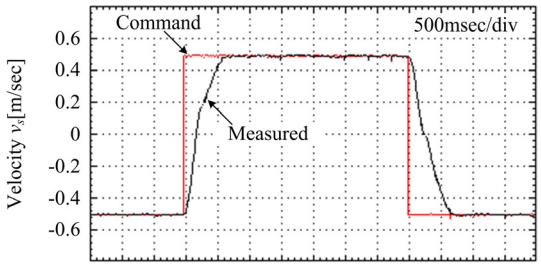

Fig. 8. Velocity response waveform.

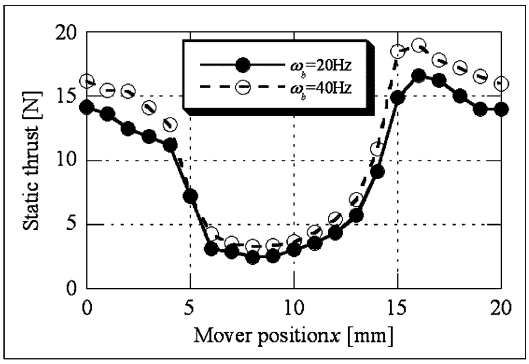

Fig. 9. Static thrust versus position characteristics.

phase of the stator. The experimental conditions were I_f = 1.0 A, I_t = 1.0 A, and the bias frequency was at 20 or 40 Hz. The generated thrust includes a component that pulsates at the bias frequency, and the measured results for each position represent an average value for this. Based on Fig. 9, the thrust pulsates significantly with respect to the position for the experimental machine. This is a thrust ripple caused by the reluctance thrust, and a motor shape that reduces this ripple must be designed. Moreover, the thrust rises a little at ω_b = 20 Hz compared to at 40 Hz. However, the authors confirmed that the period of the ripple did not vary with respect to the bias frequency.

Figure 10 shows static thrust versus I_t characteristics for I_f = 1.0 A. The thrust shown here is the average value for one period for the static thrust versus position characteristics. The rated current for the experimental machine is 4 A. If the current is increased significantly, the gap cannot be maintained because of the vertical force. As a result, measurements were taken for I_t up to 2 A. Based on the figure, the static thrust is almost proportional to I_t, that is, the static thrust in the LSM is linear with respect to I_t.

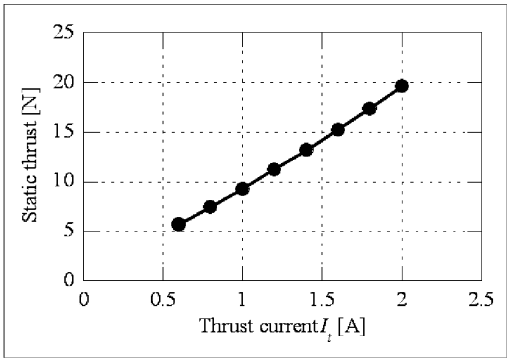

Fig. 10. Static thrust versus current characteristics.

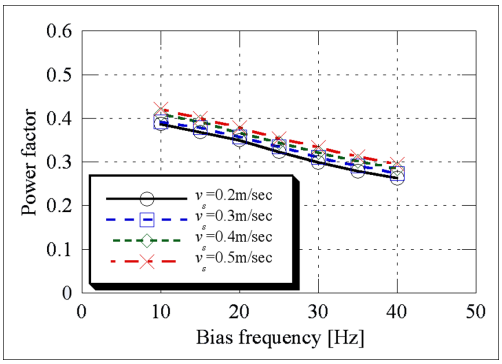

Fig. 11. Power factor versus bias frequency characteristics.

4.3 Bias frequency characteristics

Figure 11 shows the power factor versus bias frequency characteristics. The experimental conditions here were $I_f = 1.2$ A. The armature winding is set up along all stators in the experimental machine. Moreover, in half-wave rectified self-excitation, the excitation current component is provided in addition to the thrust current component to the armature winding, and as a result, the apparent power factor is in principle reduced.

As can be seen in Fig. 11, as the bias frequency increases, the power factor falls. This is thought to be because as the bias frequency increases, the phase voltage effective value for the armature winding rises. Therefore, selecting a lower limit for the bias frequency so that the pulsating frequency of the thrust is allowed is preferable for the apparent power factor.

Note that the LSM in principle includes a thrust pulsation whose bias frequency is the base wave, and as a result, when considering use in a servo system that requires high-speed response, the bias frequency must be selected so that it is sufficiently large compared to the mechanical oscillation frequency. Consequently, when using the long armature type as in this experimental machine, the stator must be set up so that the leakage inductance in the stator is reduced and a high bias frequency can be selected by altering the feeder section based on the position of the mover.

5. Characteristics Formula

Here, the authors derive a relational equation for the design parameters and characteristics for use in design and control.

5.1 Magnetic field winding current

When the diode inserted in the field winding is on, the following equation holds for the field winding voltage in Eq. (1):

$$p\lambda_{fd} + r_{fd} i_{fd} = 0 \tag{8}$$

By solving the differential equation for Eq. (8), the field winding current i_{fd} becomes

$$(0 \le \omega_b t \le \pi)$$

$$i_{fd} = \frac{3\sqrt{2}}{\pi}\omega_b T_{d0}\frac{M_{fd}}{L_{fd}} I_f \left(1 - e^{-\frac{\omega_b t}{\omega_b T_{d0}}}\right) \tag{9}$$

$$(\pi \le \omega_b t \le \omega_b \tau_1)$$

$$i_{fd} = \frac{3\sqrt{2}}{\pi}\omega_b T_{d0}\frac{M_{fd}}{L_{fd}} I_f \left(1 - e^{-\frac{\pi}{\omega_b T_{d0}}}\right) e^{-\frac{\omega_b t - \pi}{\omega_b T_{d0}}} - \frac{3\sqrt{2}}{\pi}\omega_b T_{d0}\frac{M_{fd}}{L_{fd}} I_f \left(1 - e^{-\frac{\omega_b t - \pi}{\omega_b T_{d0}}}\right) \tag{10}$$

Here, T_{d0} represents the circuit time constant for the field winding, and $\omega_b\tau_1$ is the time from when the diode is turned on and the field current starts to flow to when it reaches zero. It is given by

$$\omega_b \tau_1 = \omega_b T_{d0} \ln\left(2e^{\frac{\pi}{\omega_b T_{d0}}} - 1\right) \tag{11}$$

5.2 Thrust

First, the thrust characteristics of the LSM were explained using Eq. (6), which ignored the field winding resistance. In practice, the field winding resistance exists. As a result, the field winding current derived the thrust for the period in which Eqs. (9) and (10) are zero and the diode is off. Substituting i_{fd} in this period with λ_d in Eq. (2) and then deriving the thrust using Eq. (5) results in the following:

$$(0 \le \omega_b t \le \pi)$$

$$F = 3\sqrt{6}\frac{\pi}{\tau} I_f I_t \left[\frac{L_d - L_q}{2} - \frac{\omega_b T_{d0}}{\pi} \times \left\{(L_d - L_q)\frac{\omega_b t}{\omega_b T_{d0}} - (1-\sigma)L_d\left(1 - e^{-\frac{\omega_b t}{\omega_b T_{d0}}}\right)\right\}\right] \tag{12}$$

$$(\pi \le \omega_b t \le \omega_b \tau_1)$$

$$F = 3\sqrt{6}\frac{\pi}{\tau} I_f I_t \left[\frac{\omega_b T_{d0}}{\pi}\left\{(L_d - L_q)\frac{\omega_b t}{\omega_b T_{d0}} - (1-\sigma)L_d \times \left(e^{-\frac{\omega_b t}{\omega_b T_{d0}}} - 2e^{-\frac{\omega_b t + \pi}{\omega_b T_{d0}}}\right)\right\} - \frac{3}{2}(L_d - L_q) - \frac{\omega_b T_{d0}}{\pi}(1-\sigma)L_d\right] \tag{13}$$

$$(\omega_b \tau_1 \le \omega_b t \le 2\pi)$$

$$F = 3\sqrt{6}\frac{\pi}{\tau} I_f I_t (L_d - L_q)\left(\frac{1}{\pi}\omega_b t - \frac{3}{2}\right) \tag{14}$$

Finding the average thrust F_{avg} using Eqs. (12) through (14) results in

$$F_{avg} = 3\sqrt{6}\frac{\pi}{\tau}\omega_b T_{d0}(1-\sigma)L_d I_f I_t \left\{\frac{1}{\pi} - \frac{\omega_b T_{d0}}{2\pi^2}\ln\left(2e^{\frac{\pi}{\omega_b T_{d0}}} - 1\right)\right\} \tag{15}$$

5.3 Input power

The input power P_{in} is given by

$$P_{in} = \frac{1}{T}\int_0^T (e_d i_d + e_q i_q)dt \tag{16}$$

Here, T represent the period of $A_f(t)$.

If Eqs. (1) and (4) are substituted into Eq. (16) and $T = 2\pi/\omega_b$, then P_{in} can be written as

$$\begin{aligned} P_{in} = {} & 3\sqrt{6}\frac{\pi}{\tau}v_s\omega_b T_{d0}(1-\sigma)L_d I_f I_t \left\{\frac{1}{\pi} - \frac{\omega_b T_{d0}}{2\pi^2}\ln\left(2e^{\frac{\pi}{\omega_b T_{d0}}} - 1\right)\right\} \\ & + \frac{9}{\pi^3}\omega_b(\omega_b T_{d0})^2(1-\sigma)L_d I_f^2 \left\{\frac{\omega_b \tau_1}{\omega_b T_{d0}} - 2\left(1 - e^{-\frac{\pi}{\omega_b T_{d0}}}\right)\right\} \\ & + 3r_a\left(I_t^2 + \frac{1}{2}I_f^2\right) \end{aligned} \tag{17}$$

In Eq. (17), the first element on the right is the product of the thrust and velocity, in other words the output, and the second element on the right is cumulative energy of the inductance, and the third element on the right represents the copper loss.

5.4 Comparison of the calculated values and experimental values

When performing the calculations, the winding resistance, inductance, and other motor parameters used the values measured in the experiments. The winding resistance was measured using the voltage drop-down method, and the inductance was measured using commercial alternating current (60 Hz). The results were then converted to the dq axis inductance.

Figure 12 shows the field winding current waveform for I_f = 1.0 A and a bias frequency of 20 Hz. The experimental values match the calculated values in Eqs. (9) and (10) well.

Figure 13 shows the thrust versus I_t characteristics for I_f = 1.0 A and a bias frequency of 20 Hz. The measured values are for static thrust. The measured values and the calculated values from Eq. (15) match well when I_t is low, but as I_t increases, the error rises. This is thought to be because the gap length decreases and the measured values for the thrust characteristics increase due to an increase in vertical force as I_t rises.

Figure 14 shows the input power versus I_t characteristics for v_s = 0.3 m/s, I_f = 1.2 A, and a bias frequency of 20 Hz. The calculated values from Eq. (17) match the measured values well.

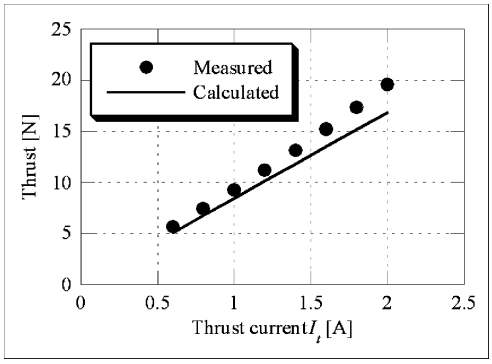

Fig. 13. Comparison of calculated and measured thrust versus current characteristics.

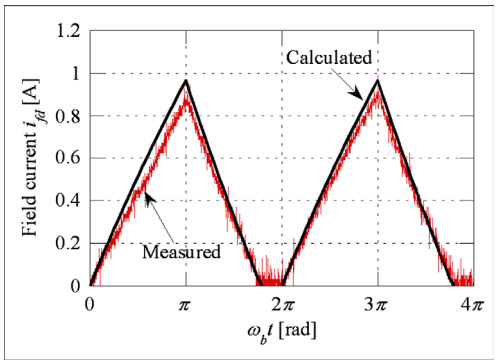

Fig. 12. Comparison of calculated and measured field current waveforms.

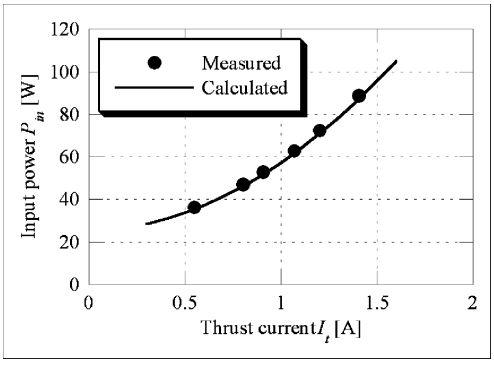

Fig. 14. Comparison of calculated and measured input power versus current characteristics.

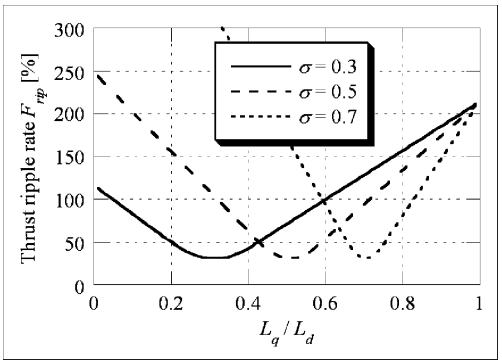

Fig. 15. Relation between thrust ripple rate and design parameters.

5.5 Relationship of thrust ripple and design parameters

Based on the above, the calculated values and measured values match well. Thus, the authors demonstrate the relationship between the design parameters and the thrust ripple due to the bias frequency as an example of using the characteristics formulas. With Eqs. (12) through (14), they calculate the thrust, then define the thrust ripple rate F_{rip} using the following equation, where the maximum value is F_{max} and the minimum value is F_{min}:

$$F_{rip} = \frac{F_{\max} - F_{\min}}{F_{avg}} \times 100 \quad [\%] \tag{18}$$

Figure 15 shows the F_{rip}–L_q/L_d characteristics where the parameter is the leakage coefficient σ. The condition here is $\omega_b T_{d0} = 20$ rad. Based on the figure, it is clear that F_{rip} reaches a minimum at $\sigma = L_q/L_d$, and as the difference between σ and L/L_d increases, F_{rip} rises. Moreover, even for the same difference between σ and L_q/L_d, the smaller σ is, the smaller F_{rip} becomes. Therefore, the thrust ripple can be reduced by setting σ and L_q/L_d to similar values, and σ to a small value.

6. Conclusion

The authors proposed a "linear synchronous motor with half-wave rectified self-excitation," a new LSM with self-excitation and a variable field flux using half-wave rectified self-excitation. They then created an experimental machine and drive system, and confirmed the drive characteristics and basic characteristics. Moreover, they derived characteristics formulas for the LSM for use in design and control, and confirmed through comparisons with measured results that the characteristics matched. Finally, they clarified the relationship between the design parameters and thrust ripple using the characteristics formulas.

REFERENCES

1. Mizuma T. Application of linear motors for transportation systems. Proc 2001 JIAS Conf, Vol. 3, No. S9-4, p 1082–1087. (in Japanese)
2. Murai M. The development of HSST system. Proc 2005 JIAS Conf., Vol. 3, No. 3-S7-2, p III69–III72. (in Japanese)
3. Karita M. Trends of linear drive technologies in industry applications. Trans IEE Japan 1999;119-D:276–278. (in Japanese)
4. Oyama J, Higuchi T, Abe T, Tanaka H, Yamada E. A novel linear synchronous motor with half-wave rectified self excitation. Third International Symposium on Linear Drives for Ind. Appl., p 144–148, Nagano, Japan, 2001.
5. Oyama J, Toba S, Higuchi T, Yamada E. The principle and fundamental characteristics of half-wave rectified brushless synchronous motor. Trans IEE Japan 1987;107-D:1257–1264. (in Japanese)
6. Oyama J, Higuchi T, Abe T, Kubota S, Hirayama T. Experimental linear synchronous motor with half-wave rectified self excitation. 14th Symposium on Electromagnetics and Dynamics, No. 3A14, p 301–306, 2002. (in Japanese)
7. Oyama J, Higuchi T, Abe T, Kubota S, Hirayama T. Principle and analysis of a novel linear synchronous motor with half-wave rectified self excitation. 17th International Conference on Magnetically Levitated Systems and Linear Drives, No. PP07109, Lausanne, Switzerland, 2002.
8. Oyama J, Higuchi T, Abe T, Yamada E. Characteristics analysis of half-wave rectified brushless synchronous motor with permanent magnets. Trans IEE Japan 1993;113-D:238–246. (in Japanese)

AUTHORS (from left to right)


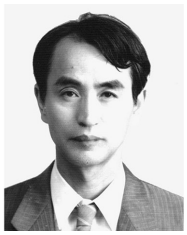

Tadashi Hirayama (student member) completed the first half of his doctoral studies in electrical engineering and computer science at Nagasaki University in 2004 and began the second half of his doctoral studies in systems science.

Jun Oyama (member) completed his doctoral studies in electrical engineering at Kyushu University in 1969 and became a lecturer on the Faculty of Engineering. He has been a professor there since 1981. He is primarily pursuing research related to power electronics and electric motor control. He holds a D.Eng. degree, and is a member of IEEE and AEM Japan.

Tsuyoshi Higuchi (member) completed his doctoral studies in electrical engineering at the Graduate School at Kyushu University in 1982 and became an instructor on the Faculty of Engineering at Nagasaki University. He was appointed an associate professor in 1984. He is primarily pursuing research related to the design of linear induction motors, and research related to power electronics and electric motor control. He holds a D.Eng. degree and is a member of AEM Japan.

Takashi Abe (member) completed a master's in electrical engineering at Nagasaki University in 1990 and then became an instructor on the Faculty of Engineering. He is primarily pursuing research related to power electronics and electric motor control. He holds a Ph.D. (engineering) degree, and is a member of IEEE and AEM Japan.